Inorganic Chemistry

Article

pubs.acs.org/IC

Effect of Metal Coordination on Photocurrent Response Properties of a Tetrathiafulvalene Organogel Film

Shu-Fang Ji,[†] Yong-Gang Sun,[†] Peng Huo,[†] Wei-Chun Shen,[†] Yu-De Huang,[†] Qin-Yu Zhu,*[,†,‡] and Jie Dai*[,†,‡]

[†]College of Chemistry, Chemical Engineering and Materials Science, Soochow University, Suzhou 215123, P. R. China

[‡]State Key Laboratory of Coordination Chemistry, Nanjing University, Nanjing 210093, P. R. China

Supporting Information

ABSTRACT: Organic low molecular weight gelators with a tetrathiafulvalene (TTF) unit have received considerable attention because the formed gels usually exhibit redox active response and conducting or semiconducting properties. However, to our knowledge, metal coordination systems have not been reported for TTF-derived gels up to date. We have designed and synthesized a series of TTF derivatives with a diamide-diamino moiety that can coordinate to specific metal ions with square coordination geometry. Gelation properties and morphologies of the films prepared by the gelators in different hydrophobic solvents are characterized. The TTF derivative with a dodecyl group shows effective gelation properties, and electrodes with the organogel films are prepared. The effect of the Ni(II) and Cu(II) coordination on the photocurrent response property of the electrodes is examined. The metal square coordination significantly increases the photocurrent response. This gel system is the first metal coordination related TTF-gel-based photoelectric material. The mechanism of the metal coordination-improved photocurrent response property is discussed based on the crystal structural analysis and theoretical calculations.

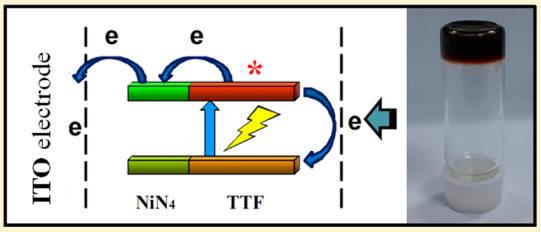

INTRODUCTION

Current interest in supramolecular gels assembled by low molecular weight gelators (LMWGs) is growing rapidly. On the basis of the low molecular weight, LMWGs are comparatively easy to intelligently design. This simplicity in turn allows potential applications of LMWGs in areas such as sensing, drug delivery, and molecular electronics.[1] Organic LMWGs with tetrathiafulvalene (TTF) units have received considerable attention because the TTF moiety can be oxidized reversibly to the corresponding radical cation and dication species sequentially,[2] and therefore (i) the formed gels may exhibit redox active responses and (ii) conducting or semiconducting nanostructures may be generated subsequently.[3] Several TTF-based organic gelators have been reported by a number of groups, and the gelation properties and resulting nanostructures have been investigated in recent decades.[4] Redox responsive gels with LMWGs featuring TTF units can be reversibly transferred between sol and gel states by inorganic or organic redox reagents, such as Fe(III) and Pb(II) ions, TCNQs (7,7,8,8-tetracyanoquinodimethane) and quinones, or electrochemical techniques.[5] Therefore, the TTF group in these organic gels, xerogels, and films can be triggered into the preparation of electronic materials.[6] By incorporation of photoresponsive chemically active segments into the respective electroactive-LMWGs, a number of photostimuli-responsive TTF gels were prepared. For instance, TTF-LMWGs with photoresponsive azobenzene and stilbene can lead to gels responding to light and redox reactions, respectively.[5b,c]

On the other hand, LMWGs which could coordinate to metal ions were obtained by using gelators containing specific moieties that can selectively bind the corresponding metal ions.[1b] For instance, a reversible sol−gel phase transition for a coordination LMWG was found possible by changing the redox state of the metal complexes.[7] The metal ion can act as a linker between LMWGs or only as a coordination component but not directly involved in linking LMWG molecules together. Incredibly, although a large number of metal coordination compounds with TTF ligands have been prepared,[8,9] based on our knowledge, metal ion coordinated TTF-based gels have not been reported yet. The reported function of metal ions in those metal ion involved TTF-based gels is only as the oxidation reagents.[5]

Here, we newly designed and synthesized a series of redox active TTF derivatives (**L1**−**L3**, Chart 1) with a diamide-diamino moiety that can selectively coordinate to specific metal

Chart 1. Compounds L1−L3

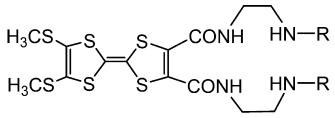

R = C_4H_9(**L1**), C_8H_{17} (**L2**), $C_{12}H_{25}$ (**L3**)

Received: December 19, 2013
Published: March 20, 2014

   dx.doi.org/10.1021/ic403107v | *Inorg. Chem.* 2014, 53, 3611−3617

ions with square coordination geometry. Gelation properties of these compounds in hydrophobic solvents and morphologies of the films prepared by the gelators are characterized. The coordination of Ni(II) or Cu(II) with the diamide-diamino moiety of the gelator significantly improves the photocurrent response property of the gelator/ITO electrode. This metal-organo gel system is the first metal coordination related TTF-gel based photoelectric material. The coordination structures of the model compounds are characterized, and the conjugated structure of the square coordination center with a TTF moiety is significant to the photocurrent conversion.

EXPERIMENTAL SECTION

General Remarks. All analytically pure reagents were purchased commercially and used without further purification. The precursor 2,3-bis(methyl-carboxylate)-6,7-bimethylthio-tetrathiafulvalene, DMT-TTF-$(CO_2Me)_2$, was prepared according to the literature methods,[10a,b] and the *N*-alkyl ethylendiamines were synthesized by reacting ethylenediamine with various halohydrocarbons.[10c] Elemental analyses of C, H, and N were performed using a VARIDEL III elemental analyzer. The FT-IR spectra were recorded as KBr pellets on a Nicolet Magna 550 FT-IR spectrometer. ^{1}H NMR spectra were measured in $CDCl_3$ using tetramethylsilane, $Si(CH_3)_4$, as an internal standard on UNITYNOVA-400 spectrophotometer. Room-temperature optical diffuse reflectance spectra of the microcrystal samples were obtained with a Shimadzu UV-3150 spectrometer, by using $BaSO_4$ powder as a reflectance reference. Room-temperature X-ray diffraction data and energy dispersive spectroscopy (EDS) were collected on a D/MAX-3C diffractometer using a Cu tube source (Cu Kα, λ = 1.5406 Å). The morphologies of the resulted films were observed with a JSM-5600LV scanning electron microscope (SEM). Cyclic voltammetry (CV) experiments were performed on a CHI650 electrochemistry workstation in a three-electrode system, a **L3** coated ITO plate working electrode, a Pt wire auxiliary electrode, a saturated calomel electrode (SCE) as a reference electrode, and 0.1 mol·L^{-1} Bu_4NClO_4 as the supporting electrolyte.

Synthesis of Compound DMT-TTF-(CONHCH$_2$CH$_2$NHC$_n$H$_{2n+1}$)$_2$ (L1, *n* = 4; L2, *n* = 8; L3, *n* = 12). The synthetic methods of the three compounds are similar. Take **L3** as a representative: A CH_3CN (15 mL) solution of DMT-TTF-$(CO_2Me)_2$ (0.206 g, 0.48 mmol) reacted with an excess of *N*-dodecyl ethylenediamine (0.456 g, 2 mmol) in 15 mL of methanol solution. After stirring for 8 h at room temperature, a precipitate formed and was collected by filtration. The precipitate was washed by CH_3CN and CH_3OH in turn and dried in vacuo to give dark-purple product **L3**, 0.20 g (50.9%). $C_{38}H_{68}N_4O_2S_6$ (805.34) calcd: C, 56.67; H, 8.51; N, 6.96. Found: C, 56.54; H, 8.49; N, 6.70. ^{1}H NMR (400 MHz, $CDCl_3$, δ): 8.39 (s, 2H, amide), 3.39 (t, J = 5.8 Hz, 4H, en), 2.80 (t, J = 5.8 Hz, 4H, en), 2.60 (t, J = 7.0 Hz, 4H, CH_2 of dodecyl), 2.42 (s, 6H, SCH_3), 1.25 (m, 40H, CH_2 of dodecyl), 0.87 (t, J = 6.4 Hz, 6H, CH_3 of dodecyl). IR (KBr): 3261b, 2918vs, 2852s, 1655m, 1575w, 1458w, 1288w, 1132w, 810w, 722w cm^{-1}. Similarly, for orange-yellow product **L1**, 0.17 g (60.1%). $C_{22}H_{36}N_4O_2S_6$ (580.91) calcd: C, 45.49; H, 6.25; N, 9.64. Found: C, 45.35; H, 6.23; N, 9.40. ^{1}H NMR (400 MHz, $CDCl_3$, δ): 8.35 (s, 2H, amide), 3.39 (t, J = 5.8 Hz, 4H, en), 2.80 (t, J = 5.8 Hz, 4H, en), 2.61 (t, J = 7.0 Hz, 4H, CH_2 of butyl), 2.42 (s, 6H, SCH_3), 1.47 (m, 4H, CH_2 of butyl), 1.37 (m, 4H, CH_2 of butyl), 0.92 (t, J = 7.2 Hz, 6H, CH_3 of butyl). IR (KBr): 3255m, 2954s, 2926s, 2828m, 1640vs, 1572s, 1461w, 1293m, 1119m, 783w cm^{-1}. Similarly, for purple product **L2**, 0.18 g (53.9%). $C_{30}H_{52}N_4O_2S_6$ (693.13) calcd: C, 51.99; H, 7.56; N, 8.08. Found: C, 51.94; H, 7.54; N, 8.07. ^{1}H NMR (400 MHz, $CDCl_3$, δ): 8.37 (s, 2H, amide), 3.39 (t, J = 6.0 Hz, 4H, en), 2.80 (t, J = 6.0 Hz, 4H, en), 2.60 (t, J = 6.6 Hz, 4H, CH_2 of octyl), 2.42 (s, 6H, SCH_3), 1.48 (m, 4H, CH_2 of octyl), 1.28 (m, 20H, CH_2 of octyl), 0.88 (t, J = 6.2 Hz, 6H, CH_3 of octyl). IR (KBr): 3308m, 2920vs, 2850s, 1649vs, 1539s, 1475m, 1411m, 1377w, 1296s, 881w, 810w cm^{-1}.

Synthesis of Compound [Ni(L1)] (1). A DMF solution (2 mL) of $Ni(OAc)_2$ (5.0 mg, 0.02 mmol) was placed into the underlayer of a glass tube. An acetonitrile solution (4 mL) of **L1** (5.8 mg, 0.01 mmol) was put into the superstratum dropwise carefully. The orange single crystals of **1** were obtained in 3 days by slow diffusion at room temperature and were used for all measurements (yield: 2.0 mg, 31.5%). $C_{22}H_{34}N_4NiO_2S_6$ (637.64) calcd: C, 41.44; H, 5.37; N, 8.79. Found: C, 41.42; H, 5.21; N, 8.71. IR (KBr): 3195w, 2960w, 2857w, 1566vs, 1461w, 1380m, 1247w, 894w, 770m, 729w cm^{-1}.

Synthesis of the Compound [Cu(L1)(DMF)] (2). A DMF solution (4 mL) of $Cu(OAc)_2$ (10.0 mg, 0.04 mmol) was placed into the underlayer of a glass tube. A acetonitrile solution (4 mL) of **L1** (5.8 mg, 0.01 mmol) was put into the superstratum dropwise carefully. The dark blue single crystals of **2** were obtained in 5 days by slow diffusion at room temperature and were used for all measurements (yield: 2.0 mg, 29.6%). $C_{25}H_{41}N_5CuO_3S_6$ (715.58): calcd: C 41.96, H 5.78, N 9.79; found: C 41.92, H 5.55, N 9.76; IR (KBr), 3216b, 2924m, 2363w, 1654m, 1573vs, 1438w, 1372s, 1028m, 759w, 610w, 475w cm^{-1}.

X-Ray Crystallographic Study. The measurements were carried out on a Rigaku Mercury CCD diffractometer with graphite monochromated Mo Kα (λ = 0.71075 Å) radiation. X-ray crystallographic data for all of the compounds were collected and processed using CrystalClear (Rigaku). The structures were solved by direct methods using the SHELXS-97 program, and the refinement was performed against F^2 using SHELXL-97.[11] All of the non-hydrogen atoms are refined anisotropically. The hydrogen atoms are positioned with idealized geometry and refined with fixed isotropic displacement parameters, while the H atoms attached to N2 and N4 of **1** were located in the Fourier maps. Detailed crystal data and structural refinement parameters for **1** and **2** are listed in Table S1 (Supporting Information).

Film Preparation and Photocurrent Measurement. Films of **L2** and **L3** were prepared using the solution coating method. A weighed amount of the new prepared compound **L2** or **L3** in a selected solvent was heated until the compound was dissolved. The hot solution was transferred to a glass syringe and then dropped on the cleaned glass plate for SEM measurement, or ITO glass (100 Ω/□; solvent: toluene) for CV and photocurrent measurements. The coating film was obtained after the solvent was carefully removed under reduced pressure. The metal ion treated electrodes were prepared by immersing the L3 electrode in $Cu(OAc)_2$, $Ni(OAc)_2$, and $Fe(ClO_4)_3$ aqueous solutions (0.10 mol·L^{-1}) for 5 days and then rinsed and dried for measurements (***Caution!*** *All metal perchlorates must be regarded as potentially explosive. Only a small amount of compound should be prepared, and it should be handled with caution*). A 150-W high pressure xenon lamp, positioned 15 cm from the surface of the ITO electrode, was employed as

dx.doi.org/10.1021/ic403107v | Inorg. Chem. 2014, 53, 3611−3617

a light source. The photocurrent experiments were parallelly performed on a CHI650 electrochemistry workstation in a three-electrode system, the sample coated (in Φ = 0.8 cm area) ITO glass as the working electrode, a Pt wire auxiliary electrode, and a saturated calomel electrode (SCE) as the reference electrode. An aqueous solution of Na_2SO_4 (200 mL, 0.1 mol·L^{-1}) was used as the medium in a quartz cell.

Computation Methods. DFT calculations were carried out using the Gaussian 09 program package.[12] Throughout the calculations, the long alkyl chains on TTF units have been replaced by methyl groups in order to cut the computational cost with no significant change in the electronic properties of TTF.[13] The compound with methyl groups, DMT-TTF-$(CONHCH_2CH_2NHCH_3)_2$, is denoted as LMe. The calculations for LMe and [Ni(LMe)] were performed by using spin-restricted DFT wave functions B3LYP. The radical ion of $LMe^{\bullet+}$ was treated as an open-shell system and was computed by using spin-unrestricted DFT wave functions UB3LYP. The basis set used for C, N, O, S, and H atoms was 6-31+G**, while effective core potentials with a LanL2DZ basis set were employed for the Ni atom.[14] The calculated energy levels of LMe, [Ni(LMe)], and $LMe^{\bullet+}$ compounds are listed in Table S2 (Supporting Information).

RESULTS AND DISCUSSION

Gelation Property and Film Morphologies of L2 and L3. We have synthesized a cation and anion sensitive system based on a TTF derivative with a diamide-diamino moiety, a similar compound to this system but the amine is not alkylated,[15] and there exist strong N−H···O hydrogen bonds in the molecular packing structure that is a basic character for a gelator. As a continued work, we designed a series of derivatives of this ligand by connecting with a long alkyl chain (butyl, octyl, and dodecyl groups) on each amine groups with the motive to increase the gelation ability of the molecules and to investigate the property of the relative film. The **L1** is not a gelator for its short *N* substituted alkyl chain (*n*-butyl group). It is prepared for the model compound to understand the metal-**L** coordination entity. The gelation ability of **L3** (*N* substituted *n*-dodecyl group) was examined in various solvents at 18 °C, and the results are listed in Table 1. As shown in Table 1, **L3** is a moderate gelator that forms gel in alkanes or arenes. Among the solvents tested, octane is the best gelation solvent, and a dark-red gel is formed by cooling a hot solution of **L3** (36 mg·mL^{-1}) in the solvent. The reversible sol−gel transition could be achieved upon cooling and heating (Figure 1). Compound **L2** (*n*-octyl group) is also a gelator that forms a ductile gel in toluene and 1,2-dichloroethane, but the gelation ability is poorer than that of **L3** under the same conditions.

Table 1. Gelation Results in Different Solvents with L3 at 18 °C (mL^{-1})[a]

solvent	gelation	solvent	gelation
octane	G (36 mg)	dioxane	G (140 mg)
n-heptane	G (40 mg)	chloroform	S
toluene	G (54 mg)	*n*-hexane	P
benzene	G (96 mg)	ethyl acetate	P
cyclohexane	G (100 mg)	ethanol	P
1,2-dichloroethane	G (112 mg)	acetonitrile	I

[a]G, gel; S, solution; P, precipitate; I, insoluble. The critical gelator concentrations (CGCs) of the corresponding gels were measured at room temperature (~18 °C) and listed in the parentheses.

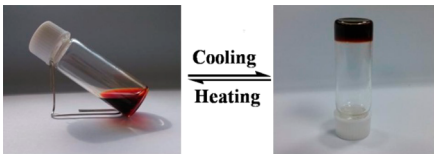

Figure 1. Illustration of the gel formation with **L3** (36 mg mL^{-1}) in octane and the sol−gel transition upon cooling and heating.

The self-assembly films of **L2** and **L3** were prepared by coating hot solutions with different solvents on a glass substrate, and then the solvents were carefully removed under reduced pressure to yield the respective films. The films were subjected to scanning electron microscope (SEM) analysis. Figure 2a−f show the SEM images of the morphologies obtained in different solvents. Interconnected belt-like microstructures, being typical of the organogels, were observed. On the basis of the SEM images, the gelation property clearly relates to the microstructures of the gels. The gel of **L3** is selected as a representative example. In the case of toluene (Figure 2a), a porous interlocked network of fibers (1 μm in width) is observed. In the case of cyclohexane, though the fibers seem similar to those in toluene, they are bundled, and large voids are formed (Figure 2b) so that the solvent molecules are more easily lost than the former. The fibers are almost fused forming a film structure with larger holes in 1,2-dichloroethane, and less solvent can be fixed (Figure 2c). Therefore, the gelation ability of **L3** in these three solvents is in the following order: toluene > cyclohexane > 1,2-dichloroethane. While, in chloroform, the **L3** can only form a smooth film with some holes (Figure 2d). The SEM images of **L2** in toluene and cyclohexane are given in Figure 2e and f, respectively. In comparison with **L3** in the same solvents, these belts are further broadened and fused, which have less effective network voids for solvent molecules included. The **L1** can only form a smooth film or fused microstructure in toluene and cyclohexane, respectively (Figure S1).

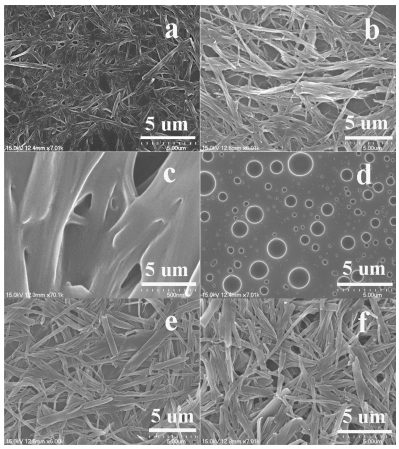

Figure 2. SEM images of the morphologies of the films **L3** (a, toluene; b, cyclohexane; c, 1,2-dichloroethane; d, chloroform) and **L2** (e, toluene; f, cyclohexane) prepared in different solvents.

Since the TTF unit is a redox active moiety of the gelator, the redox property of the **L3** film was investigated by cyclic voltammetry (CV). The electrode was prepared by the same

dx.doi.org/10.1021/ic403107v | Inorg. Chem. 2014, 53, 3611−3617

coating method as mentioned above except that the glass substrate was replaced by an ITO plate. The CV result in a medium of CH_3CN is illustrated in Figure S2. Two redox waves were detected with $E_{1/2}(1)$ and $E_{1/2}(2)$ at 0.588 and 0.853 V, respectively, corresponding to the $TTF^{\bullet+}/TTF$ and $TTF^{2+}/TTF^{\bullet+}$ redox couples. The relatively lower first step oxidation potential indicates that the electrode should be of easy electron loss.

Transition Metal Ion Coordinated L3 Films. The previous research work indicated that the TTF derivative with a diamide-diamino moiety selectively coordinates to Cu(II) and Ni(II) ions forming redox active complexes.[15] To investigate the effect of the metal coordination on the **L3** film, Ni(II), Cu(II), and Fe(III) treated **L3** films were prepared. The Fe(III) was selected as a comparing ion, because it was not coordinated by this type of ligand.[15] The octahedral coordination Fe(III) or Fe(II) ion cannot enter the diamide-diamino coordination center due to the diamide-diamino environment being only in favor of the square coordination ions. The EDS data reveal that the element ratios of S/Ni and S/Cu are 10:1 and 16:2, respectively, for the Ni(II) and Cu(II) treated films. No Fe(III) was detected for the Fe(III) treated film; instead, a Cl signal appeared (Figure S3). On the basis of the knowledge of TTF chemistry and previous research, it is reasonable that the **L3** film is oxidized by the Fe(III) ion.[16] IR and UV–vis absorption spectra were measured to further confirm the result (Figure 3). The IR signals of amino and

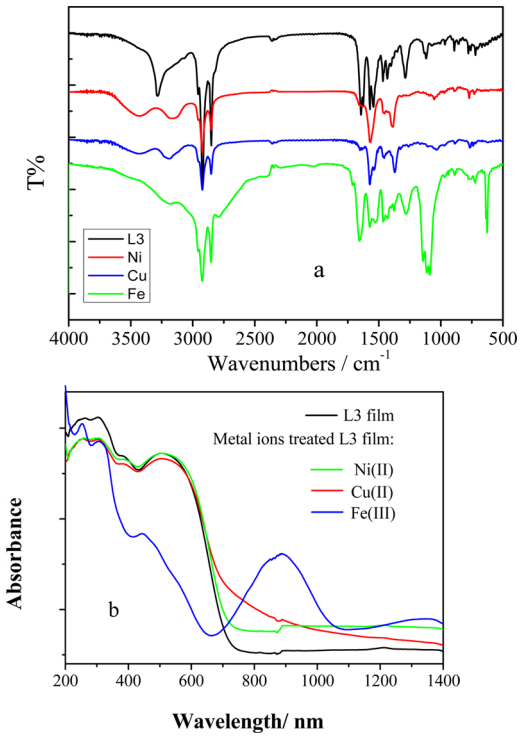

Figure 3. (a) IR and (b) UV–vis absorption spectra of an **L3** film and of Ni(II), Cu(II), and Fe(III) treated **L3** films.

amido groups are shifted due to the Ni(II) and Cu(II) coordination. The spectrum of the Fe(III) treated film is completely different from that of the **L**, and a broad and strong signal of ClO_4^- appears at 1100 cm^{-1}. The UV–vis absorption spectrum also shows that the TTF moiety is oxidized to $TTF^{\bullet+}$ due to the appearance of the characteristic absorption peak at 850 nm,[16] which is in accordance with the color change of the film. All of these results indicate that the film is oxidized in the presence of Fe(III).

Figure 4 shows the SEM images of the morphologies of the metal ion treated **L3** films (originally prepared in toluene). The

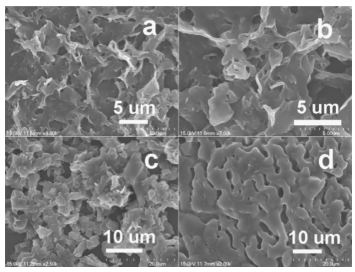

Figure 4. SEM images of the morphologies of (a) **L3** film and of (b) Ni(II), (c) Cu(II), and (d) Fe(III) treated **L3** films.

original interconnected belt-like microstructure (Figure 2a) was changed after the metal ion was treated. On the basis of the SEM images, the morphologies of Ni(II) and Cu(II) ion coordinated films show an irregular petal-like microstructure due to the bonding effect of metal coordination. The morphology of the Fe(III) ion treated film shows a fused belt microstructure that is different from the formers'. The XRD pattern of the **L3** film shows a broad peak at 20.5 eV (Figure S4). No pattern change was observed for the Ni-**L3** and Cu-**L3** films; however, the peak at 20.5 eV completely disappeared for the Fe(III) treated **L3** film. These results further support the different reaction mechanisms.

Model Coordination Complexes 1 and 2. As the model compounds to understand the structures of the metal treated **L3** films, two Ni(II) and Cu(II) complexes with **L1** were prepared and characterized crystallographically. IR and solid-state UV–vis absorption spectra were measured to confirm the identity of the films with the model compounds **1** and **2** (Figure 5). The IR spectra of the complexes **1** and **2** are similar to those of the CuL and NiL films, except the C–H stretching bands are decreased due to their short alkyl groups. The absorption spectra are in accordance with the colors of the compounds. Different from the ligand **L**, a new absorption band appears at about 700 nm for **1**[17a] and 600 nm for **2**,[17b] which can be assigned to the metal coordinaton-centered transition. Comparing the spectra in Figure 5b with those of CuL and NiL films in Figure 3b, the d–d peaks are not well-resolved in the film spectra, but the absorption edges are red-shifted.

The asymmetric units of complexes **1** and **2** are shown in Figure 6 and Figure S5. In **1**, the nickle atom is coordinated with four nitrogen atoms of the ligand (diamide-diamino moiety) and adopts a square configuration (Figure 6a). The average $Ni-N_{amide}$ distance is 1.878 Å, and the average $Ni-N_{amine}$ distance is 1.945 Å, which fall in the range of normal Ni–N bonds. The difference in the Ni–N distances means that two deprotonated amido nitrogen atoms have a stronger coordination ability than those of amino nitrogen atoms. The four nitrogen atoms are quasi-planar with a mean deviation of 0.0124(25) Å, and the nickel ion is on the plane with a deviation of 0.1328(4) Å. The average distance of $C-N_{amide}$ is 1.320 Å shorter than that of $C-N_{amine}$ (1.476 Å), showing the partial double bond character which arises from the conjugation of the amide group with the TTF moiety. The conjugation

dx.doi.org/10.1021/ic403107v | Inorg. Chem. 2014, 53, 3611–3617

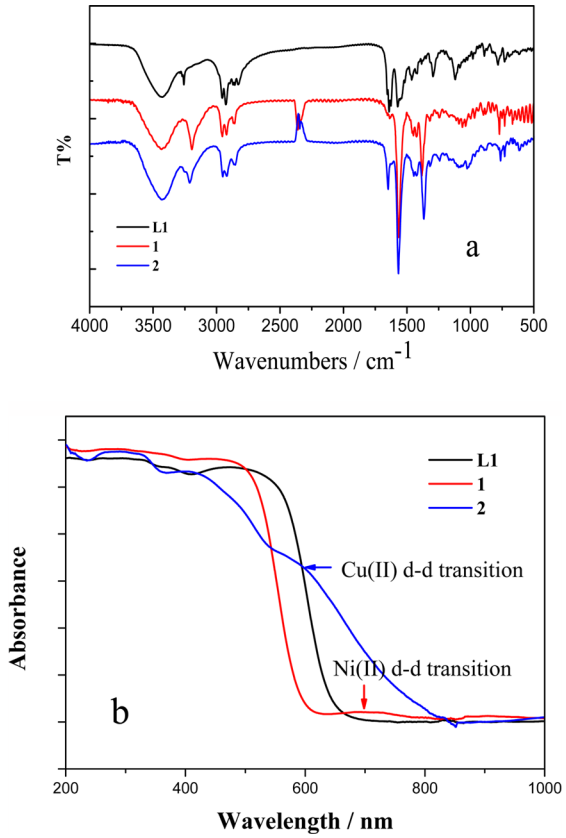

Figure 5. (a) IR and (b) solid-state UV–vis absorption spectra of **L1** and compounds **1** and **2**.

extends to the NiN_4 square plane (Figure 6c). The two alkyl chains stretch parallel in the direction perpendicular to the TTF plane. Interconnected by strong double hydrogen bonds, N–H···O···H–N, neighboring molecules form a 1-D structure with a herringbone arrangement (Figure S6), the basic character of molecular arrangement for this type of compound.[15]

The molecular structure of **2** is similar to that of **1**, except that the copper atom is five coordinated with four nitrogen atoms of the ligand and one axial oxygen atom from a weak coordinated DMF molecule, and adopts a distorted square-pyramidal configuration (Figure 6b). The average $Cu–N_{amide}$ distance is 1.965 Å, and the average $Cu–N_{amine}$ distance is 2.070 Å. The Cu–O distance of 2.274 Å is longer than those of the Cu–N distances. The four nitrogen atoms are quasi-planar with a mean deviation of 0.0045(53) Å. The Cu atom deviates from the least-squares plane of these atoms by 0.3267(12) Å and toward the axial oxygen. Similarly, the two alkyl chains extend parallelly in the direction perpendicular to the TTF moiety, but the TTF unit takes a boat conformation with serious bend that should be due to the space effect of the solvent coordination. Referring to Figure 6d and Figure S7, both sides of the TTF moiety are bent with respect to the central C_2S_4 plane by 21.1° and 23.3°, respectively, while the TTF moiety in **1** is roughly flattened, and only the coordination side bends about 15.1°. Consequently, the conjugation of the TTF moeity in **2** is not as good as that in **1**.

Photocurrent Response. To investigate the effect of metal coordination on photoelectric conversion properties, **L3**-coated ITO electrodes (**L3**/ITO) and metal-ion-treated **L3**/ITO electrodes are used as working electrodes in a photoelectrochemical cell for measurements. All of the experiments were carried out in a 0.10 mol·L^{-1} Na_2SO_4 electrolyte solution

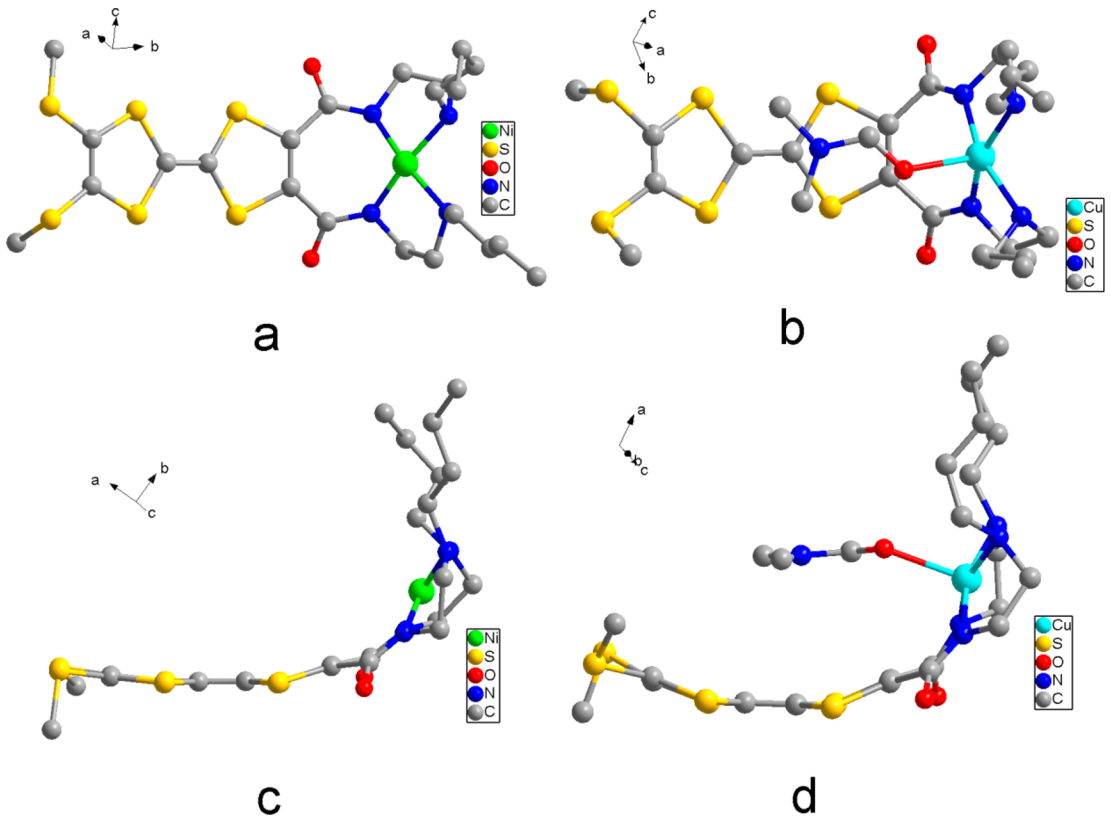

Figure 6. Molecular structures of **1** (a, c) and **2** (b, d) showing the coordination environment and the molecular profiles.

dx.doi.org/10.1021/ic403107v | Inorg. Chem. 2014, 53, 3611–3617

under irradiation with a 150-W high pressure xenon lamp (a more detailed description is given in the Experimental Section).

Figure 7 shows the photocurrent responses as the excitation light is turned on and off repeatedly. The **L3**/ITO electrode

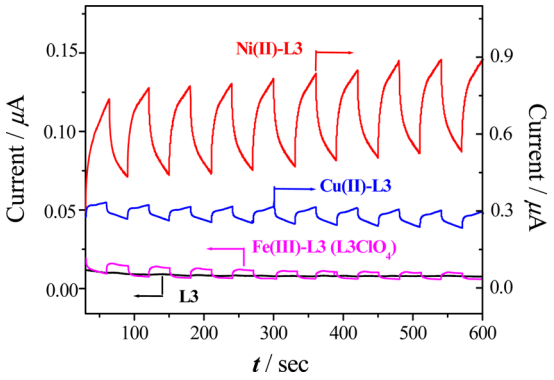

Figure 7. Photocurrent responses of the films upon repetitive irradiation, **L3** (black), Fe-**L3** (purple), Cu-**L3** (blue), and Ni-**L3** (red) (three-electrode system, sample coated ITO glass in 0.10 mol·L^{-1} aqueous solution of Na_2SO_4).

does not display any light-gated response on a 10^{-8} Å scale (Figure 7, black line), and the Ni(II) and Cu(II) treated **L3**/ITO electrodes show anodic photocurrent responses (Figure 7, blue line Cu(II)-**L3** and red line Ni(II)-**L3**). However, the Fe(III) treated **L3**/ITO electrode shows a cathodic current, and the intensity is very weak (10^{-8} Å). Because all the measurements were carried out parallelly in the same manner, the different current direction and intensity mean there are different mechanisms in electron transfer. As discussed above, the Ni(II) and Cu(II) treated **L3** electrodes form metal coordination films, while the Fe(III) treated **L3** electrode forms an oxidized **L3** film. This is the point for the different photocurrent behaviors. The metal coordination center should play an important role in promoting the photoinduced current, because the non-metal-coordinated **L3** electrode does not generate visible current. The Fe(III) treated **L3**/ITO electrode, being more correctly the **L3**ClO_4/ITO electrode, is a TTF radical material, an electroactive medium. For this reason, it shows a quick responsive cathodic current (square curve) in comparison with the others, though its photocurrent intensity is very weak.

The molecular energy levels of **LMe**, [**Ni(LMe)**], and **LMe**$^{\bullet+}$ were calculated using the Gaussian 09 program package (Table S2). Figure 8a shows schematically the HOMO and LUMO energies and the band structure of the ITO electrode. The HOMO−LUMO energy gap of [**Ni(LMe)**] is 2.4 eV narrower than that of **LMe** (3.0 eV). Therefore, the [**Ni(LMe)**] electrode shows effective photoexcitation and electron transition from LUMO (−2.0367 eV) to ITO (−4.7 eV),[18] an anodic current. The HOMO (−8.5064 eV) and LUMO (−5.2525 eV) energies of the radical **LMe**$^{\bullet+}$ drop down below the ITO energy level, and hence only the reverse electron flow is possible, a cathodic current. On the basis of the structural information, the square coordination Ni(II) ion and quasi-square coordination Cu(II) ion are coordinated into the diamide-diamino center, and the conjugated TTF and metal coordination MN_4 dyad system is formed. The molecular orbital analyses of [**Ni(LMe)**] (Figure 8b) show that the largest coefficients in the HOMO orbital are mainly localized on the central TTF core (the $S_2C{=}CS_2$ fragment), while the LUMO orbital population almost

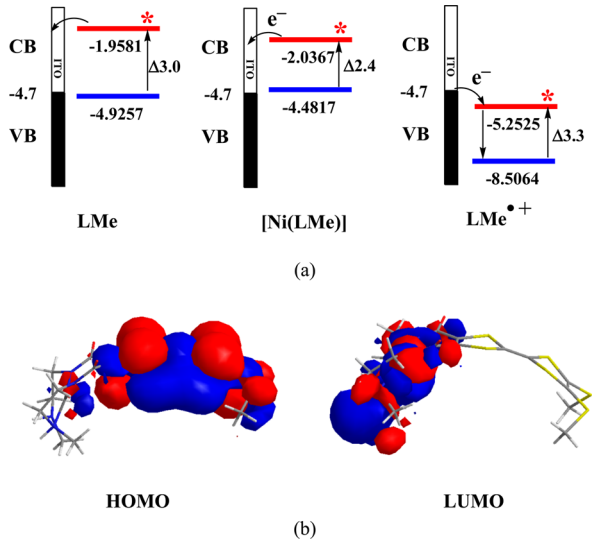

Figure 8. (a) Proposed mechanism for the photocurrent generation (all the data are in eV). (b) The calculated population coefficients of HOMO and LUMO for [**Ni(LMe)**].

completely shifts to the square coordination center NiN_4. Under irradiation, the electron transfer is from HOMO (TTF) to LUMO (NiN_4) and then from the coordination center to the electrode. This result shows the effect of the coordination center on photocurrent response, and it also settles the problem why no obvious photocurrent response for the **L3** electrode was observed. Therefore, the TTF moiety conjugated square coordination NiN_4 or CuN_4 is a photoactive cooperative system, though the role of the metal coordination centers of MN_4 needs to be further studied.

CONCLUSIONS

A series of TTF derivatives **L1**−**L3** with a diamide-diamino moiety are synthesized that can coordinate to specific metal ions with square coordination geometry, Ni(II) and Cu(II) ions. Gelation properties and film morphologies of these compounds in hydrophobic solvents are characterized. The compounds with octyl and dodecyl groups are gelators, and the dodecyl derivative shows the most effective gelation property. An interconnected belt-like microstructure is a typical morphology of the organogels, in which the most effective gelation microstructures are observed for **L3** in toluene and cyclohexane. To our knowledge, metal coordination systems have not been reported for TTF-derived gels up to date. The effect of the Ni(II) and Cu(II) coordination on the photocurrent response property is examined. The **L3** coated ITO electrode does not display an obvious response; however, the metal coordination in square mode, Ni(II)-**L3** and Cu(II)-**L3**, significantly increases the photocurrent response. A mechanism of the enhancement of photocurrent response is proposed that relates to the square metal coordination structures. This is the first targeted work to design a metal coordination related TTF-gel based material showing a metal coordination cooperative effect on photocurrent response property.

ASSOCIATED CONTENT

Supporting Information

X-ray crystallographic data of **1** and **2** in CIF format. Crystal data and structural refinement parameters for **1** and **2**. The

dx.doi.org/10.1021/ic403107v | Inorg. Chem. 2014, 53, 3611−3617

calculated energy levels of LMe, [Ni(LMe)], and $LMe^{\bullet+}$ compounds. SEM images of the morphologies of the film L1 in toluene and cyclohexane. Cyclic voltammogram of **L3** film (Bu_4NClO_4, 0.1 mol·L^{-1}, 100 mVs^{-1}) in CH_3CN. EDS results of the metal ion doped L3/ITO electrodes. XRD results of the metal ions doped L3/ITO electrodes and L3/ITO electrodes. Asymmetric structures of complexes **1** and **2**. The one-dimensional structures of **1** and **2** with herringbone arrangement molecules that interconnected by strong double hydrogen bonds, N−H···O···H−N. Side views of the molecules **1** and **2**, showing the bending of the TTF moieties. This material is available free of charge via the Internet at http://pubs.acs.org.

AUTHOR INFORMATION

Corresponding Authors

*E-mail: zhuqinyu@suda.edu.cn.

*E-mail: daijie@suda.edu.cn.

Notes

The authors declare no competing financial interest.

ACKNOWLEDGMENTS

We gratefully acknowledge financial support by the NSF of China (21171127 and 21371125), the Priority Academic Program Development of Jiangsu Higher Education Institutions, and the Program of Innovative Research Team of Soochow University.

REFERENCES

(1) (a) Ajayaghosh, A.; Praveen, V. K.; Vijayakumar, C. *Chem. Soc. Rev.* **2008**, *37*, 109−122. (b) Piepenbrock, M. O. M.; Lloyd, G. O.; Clarke, N.; Steed, J. W. *Chem. Rev.* **2010**, *110*, 1960−2004. (c) Steed, J. W. *Chem. Soc. Rev.* **2010**, *39*, 3686−3699. (d) Babu, S. S.; Prasanthkumar, S.; Ajayaghosh, A. *Angew. Chem., Int. Ed.* **2012**, *51*, 1766−1776.

(2) (a) Jørgensen, T.; Hansen, T. K.; Becher, J. *Chem. Soc. Rev.* **1994**, 41−51. (b) Segura, J. L.; Martin, N. *Angew. Chem., Int. Ed.* **2001**, *40*, 1372−1409. (c) Canevet, D.; Sallé, M.; Zhang, G.; Zhang, D.; Zhu, D. *Chem. Commun.* **2009**, 2245−2269. (d) Bryce, M. R. *J. Mater. Chem.* **2000**, *10*, 589−598. (e) Saito, G.; Yoshida, Y. *Bull. Chem. Soc. Jpn.* **2007**, *80*, 1−137. (f) Hünig, S.; Kiesslich, G.; Sceutzow, D.; Zhrandik, R.; Carsky, P. *Int. J. Sulfur Chem., Part C* **1971**, 109−122. (g) Deuchert, K.; Hünig, S. *Angew. Chem., Int. Ed.* **1978**, *17*, 875−958 and refs therein.

(3) (a) Yang, X.; Zhang, D.; Zhang, G.; Zhu, D. *Sci. China Chem.* **2011**, *54*, 596−602. (b) Amabilino, D. B.; Puigmarí-Luis, J. *Soft Matter* **2010**, *6*, 1605−1612. (c) Sui, X.; Feng, X.; Hempenius, M. A.; Vancso, G. J. *J. Mater. Chem. B* **2013**, *1*, 1658−1672.

(4) (a) Akutagawa, T.; Kakiuchi, K.; Hasegawa, T.; Noro, S.; Nakamura, T.; Hasegawa, H.; Mashiko, S.; Becher, J. *Angew. Chem., Int. Ed.* **2005**, *44*, 7283−7287. (b) Puigmartí-Luis, J.; Pino, Á. P.; Laukhin, V.; Feldborg, L. N.; Rovira, C.; Laukhina, E.; Amabilino, D. B. *J. Mater. Chem.* **2010**, *20*, 466−474. (c) Kitamura, T.; Nakaso, S.; Mizoshita, N.; Tochigi, Y.; Shimomura, T.; Moriyama, M.; Ito, K.; Kato, T. *J. Am. Chem. Soc.* **2005**, *127*, 14769−14775. (d) Kitahara, T.; Shirakawa, M.; Kawano, S-i.; Beginn, U.; Fujita, N.; Shinkai, S. *J. Am. Chem. Soc.* **2005**, *127*, 14980−14981. (e) Zhao, Y.-L.; Aprahamian, I.; Trabolsi, A.; Erina, N.; Stoddart, J. F. *J. Am. Chem. Soc.* **2008**, *130*, 6348−6350.

(5) (a) Wang, C.; Zhang, D.; Zhu, D. *J. Am. Chem. Soc.* **2005**, *127*, 16372−16373. (b) Yang, X.; Zhang, G.; Li, L.; Zhang, D.; Chi, L.; Zhu, D. *Small* **2012**, *8*, 578−584. (c) Wang, C.; Chen, Q.; Sun, F.; Zhang, D. Q.; Zhang, G. X.; Huang, Y. Y.; Zhao, R.; Zhu, D. B. *J. Am. Chem. Soc.* **2010**, *132*, 3092−3096.

(6) (a) Puigmartí-Luis, J.; Laukhin, V.; Pino, Á. P.; Vidal-Gancedo, J.; Rovira, C.; Laukhina, E.; Amabilino, D. B. *Angew. Chem., Int. Ed.* **2007**, *46*, 238−241. (b) Puigmartí-Luis, J.; Laukhina, E.; Laukhin, V.; Pino, Á. P.; Mestres, N.; Vidal-Gancedo, J.; Rovira, C.; Amabilino, D. B. *Adv. Funct. Mater.* **2009**, *19*, 934−941.

(7) (a) Kawano, S.; Fujita, N.; Shinkai, S. *J. Am. Chem. Soc.* **2004**, *126*, 8592−8593. (b) Peng, F.; Li, G.; Liu, X.; Wu, S.; Tong, Z. *J. Am. Chem. Soc.* **2008**, *130*, 16166−16167.

(8) See for example: (a) Lorcy, D.; Bellec, N.; Fourmigué, M.; Avarvari, N. *Coord. Chem. Rev.* **2009**, *253*, 1398−1438. (b) Cosquer, G.; Pointillart, F.; Le Gal, Y.; Golhen, S.; Cador, O.; Ouahab, L. *Chem.—Eur. J.* **2011**, *17*, 12502−12511. (c) Nguyen, T. L. A.; Devic, T.; Mialane, P.; Rivière, E.; Sonnauer, A.; Stock, N.; Demir-Cakan, R.; Morcrette, M.; Livage, C.; Marrot, J.; Tarascon, J.-M.; Férey, G. *Inorg. Chem.* **2010**, *49*, 10710−10717. (d) Cai, X.-M.; Zhang, X.-Y.; Savchenko, J.; Cao, Z.; Ren, T.; Zuo, J.-L. *Organometallics* **2012**, *31*, 8591−8597. (e) Ran, Y.-F.; Liu, S.-X.; Sereda, O.; Neels, A.; Decurtins, S. *Dalton Trans.* **2011**, *40*, 8193−8198.

(9) (a) Qin, Y.-R.; Zhu, Q.-Y.; Huo, L.-B.; Shi, Z.; Bian, G.-Q.; Dai, J. *Inorg. Chem.* **2010**, *49*, 7372−7381. (b) Shao, M.-Y.; Huo, P.; Sun, Y.-G.; Li, X.-Y.; Zhu, Q.-Y.; Dai, J. *CrystEngComm* **2013**, *15*, 1086−1094. (c) Zhu, Q.-Y.; Wang, J.-P.; Qin, Y.-R.; Shi, Z.; Han, Q.-H.; Bian, G.-Q.; Dai, J. *Dalton Trans.* **2011**, *40*, 1977−1983. (d) Wang, J.-P.; Lu, Z.-J.; Zhu, Q.-Y.; Zhang, Y.-P.; Qin, Y.-R.; Bian, G.-Q.; Dai, J. *Cryst. Growth Des.* **2010**, *10*, 2090−2095.

(10) (a) Hudhomme, P.; Moustarder, S. L.; Durand, C.; Gallego-Planas, N.; Mercier, N.; Blanchard, P.; Levillain, E.; Allain, M.; Gorgues, A.; Riou, A. *Chem.—Eur. J.* **2001**, *7*, 5070−5083. (b) McCullough, R. D.; Petruska, M. A.; Belot, J. A. *Tetrahedron* **1999**, *55*, 9979−9998. (c) Lu, X.; Zhang, Z.; Liang, Y. *Langmuir* **1997**, *13*, 533−538.

(11) (a) Sheldrick, G. M. *SHELXS-97, Program for Structure Solution*; Universität of Göttingen: Göttingen, Germany. 1999. (b) Sheldrick, G. M. *SHELXL-97, Program for Structure Refinement*; Universität of Göttingen: Göttingen, Germany. 1997.

(12) Frisch, M. J.; Trucks, G. W.; Schlegel, H. B.; Scuseria, G. E.; Robb, M. A.; Cheeseman, J. R.; Scalmani, G.; Barone, V.; Mennucci, B.; Petersson, G. A.; Nakatsuji, H.; Caricato, M.; Li, X.; Hratchian, H. P.; Izmaylov, A. F.; Bloino, J.; Zheng, G.; Sonnenberg, J. L.; Hada, M.; Ehara, M.; Toyota, K.; Fukuda, R.; Hasegawa, J.; Ishida, M.; Nakajima, T.; Honda, Y.; Kitao, O.; Nakai, H.; Vreven, T.; Montgomery, J. A.; Peralta, J. E., Jr.; Ogliaro, F.; Bearpark, M.; Heyd, J. J.; Brothers, E.; Kudin, K. N.; Staroverov, V. N.; Kobayashi, R.; Normand, J.; Raghavachari, K.; Rendell, A.; Burant, J. C.; Iyengar, S. S.; Tomasi, J.; Cossi, M.; Rega, N.; Millam, J. M.; Klene, M.; Knox, J. E.; Cross, J. B.; Bakken, V.; Adamo, C.; Jaramillo, J.; Gomperts, R.; Stratmann, R. E.; Yazyev, O.; Austin, A. J.; Cammi, R.; Pomelli, C.; Ochterski, J. W.; Martin, R. L.; Morokuma, K.; Zakrzewski, V. G.; Voth, G. A.; Salvador, P.; Dannenberg, J. J.; Dapprich, S.; Daniels, A. D.; Farkas, O.; Foresman, J. B.; Ortiz, J. V.; Cioslowski, J.; Fox, D. J. *Gaussian 09*, revision A.02; Gaussian, Inc.: Wallingford, CT, 2009.

(13) Noda, M.; Misaki, Y.; Tanaka, K. *Curr. Appl. Phys.* **2006**, *6*, 943.

(14) (a) Hay, P. J.; Wadt, W. R. *J. Chem. Phys.* **1985**, *82*, 270−283. (b) Bharatia, P.; Bhartia, A.; Bharty, M. K.; Maiti, B.; Butcher, R. J.; Singh, N. K. *Polyhedron* **2013**, *63*, 156−166.

(15) (a) Lu, Z.-J.; Wang, J.-P.; Zhu, Q.-Y.; Huo, L.-B.; Qin, Y.-R.; Dai, J. *Dalton Trans.* **2010**, *39*, 2798−2803. (b) Shi, Z.; Lu, Z.-J.; Zhu, Q.-Y.; Huo, L.-B.; Han, Q.-H.; Bian, G.-Q.; Dai, J. *J. Phys. Chem. B* **2011**, *115*, 3020−3026.

(16) (a) Zhu, Q.-Y.; Han, Q.-H.; Shao, M.-Y.; Gu, J.; Shi, Z.; Dai, J. *J. Phys. Chem. B* **2012**, *116*, 4239−4247. (b) Zhu, Q.-Y.; Huo, L.-B.; Qin, Y.-R.; Zhang, Y.-P.; Lu, Z.-J.; Wang, J.-P.; Dai, J. *J. Phys. Chem. B* **2010**, *114*, 361−367.

(17) (a) Diwan, K.; Chauhan, R.; Singh, S. K.; Singh, B.; Drew, M. G. B.; Bahadura, B.; Singh, N. *New J. Chem.* **2014**, *38*, 97−108. (b) Paul, S.; Barik, A. K.; Peng, S. M.; Kar, S. K. *Inorg. Chem.* **2002**, *41*, 5803−5809.

(18) (a) Zhong, Y. L.; Midya, A.; Ng, Z.; Chen, Z.-K.; Daenen, M.; Nesladek, M.; Loh, K. P. *J. Am. Chem. Soc.* **2008**, *130*, 17218−17219. (b) Hyung, K.-H.; Noh, J.; Lee, W.; Han, S.-H. *J. Phys. Chem. C* **2008**, *112*, 18178−18182.